Digital Communications and Networks xxx (xxxx) xxx

Contents lists available at ScienceDirect

Digital Communications and Networks

journal homepage: www.keaipublishing.com/dcan

Ambient backcom in beyond 5G NOMA networks: A multi-cell resource allocation framework

Wali Ullah Khan [a,*], Fida Hussain Memon [b], Kapal Dev [c], Muhammad Awais Javed [d], Dinh-Thuan Do [e], Nawab Muhammad Faseeh Qureshi [f,**]

[a] Interdisciplinary Centre for Security, Reliability and Trust (SnT), University of Luxembourg, 1855 Luxembourg City, Luxembourg
[b] Department of Electrical Engineering Sukkur IBA University, Pakistan
[c] Department of Institute of Intelligent Systems, University of Johannesburg, South Africa
[d] Department of Electrical and Computer Engineering, COMSATS University Islamabad, 44000, Islamabad, Pakistan
[e] Electrical Engineering Department, University of Colorado Denver, Denver, CO, 80204, USA
[f] Department of Computer Education, Sungkyunkwan University, Seoul, South Korea

ARTICLE INFO

Keywords:
Beyond fifth-generation
Non-orthogonal multiple access
Ambient BackCom
Spectrum efficiency optimization

ABSTRACT

The research of Non-Orthogonal Multiple Access (NOMA) is extensively used to improve the capacity of networks beyond the fifth-generation. The recent merger of NOMA with ambient Backscatter Communication (BackCom), though opening new possibilities for massive connectivity, poses several challenges in dense wireless networks. One of such challenges is the performance degradation of ambient BackCom in multi-cell NOMA networks under the effect of inter-cell interference. Driven by providing an efficient solution to the issue, this article proposes a new resource allocation framework that uses a duality theory approach. Specifically, the sum rate of the multi-cell network with backscatter tags and NOMA user equipments is maximized by formulating a joint optimization problem. To find the efficient base station transmit power and backscatter reflection coefficient in each cell, the original problem is first divided into two subproblems, and then the closed form solution is derived. A comparison with the Orthogonal Multiple Access (OMA) ambient BackCom and pure NOMA transmission has been provided. Simulation results of the proposed NOMA ambient BackCom indicate a significant improvement over the OMA ambient BackCom and pure NOMA in terms of sum-rate gains.

1. Introduction

Next generation wireless networks demand high spectral efficiency, low energy consumption, and increased connectivity [1,2]. These networks would be heterogeneous and involve cell smart-phones, vehicles on the road, unmanned aerial vehicles in the air, and satellites in different orbits of the space, respectively [3–5]. Recently, some solutions have emerged, such as Non-Orthogonal Multiple Access (NOMA), Backscatter Communication (BackCom), intelligent reflecting surfaces, artificial intelligence, and edge computing. NOMA is a potential solution to meet these requirements in cellular networks after the fifth generation (5G) [6,7]. Its spectrum efficiency over the conventional Orthogonal Multiple Access (OMA) solutions has made it popular among both industry and academia [8,9]. Multiple users in a system using NOMA technique can access the same spectrum resources at one time [10]. The signals of these users can be successfully multiplexed at transmitters using the superposition coding technique. The decoding process takes place at the receivers using Successive Interference Cancellation (SIC) technique [11]. As a favorable technology to improve both the system capacity and user access, the applications of NOMA have been explored for Cognitive Radio (CR) [12], millimeter-Wave (mmWave) [13], and massive Multiple-Input-and-Multiple-Output (MIMO) heterogeneous networks [14]. Besides, some other studies indicate applications of NOMA for grant-free access [15], physical layer security [16], vehicular communication [17], and mobile-edge computing [18]. The rapid evolution of NOMA techniques has led to the point where researchers have started exploring their applications in BackCom.

Lately, BackCom is emerging as a power and spectrum-efficient technology to enable massive connectivity [19]. Generally, BackCom consists of two parts, i.e., an Radio Frequency (RF) source/reader and a

* Corresponding author.
** Corresponding author.
E-mail addresses: waliullah.khan@uni.lu (W.U. Khan), faseeh@skku.edu (N.M.F. Qureshi).

https://doi.org/10.1016/j.dcan.2022.10.028
Received 21 September 2021; Received in revised form 21 October 2022; Accepted 25 October 2022
Available online xxxx

Please cite this article as: W.U. Khan et al., Ambient backcom in beyond 5G NOMA networks: A multi-cell resource allocation framework, Digital Communications and Networks, https://doi.org/10.1016/j.dcan.2022.10.028

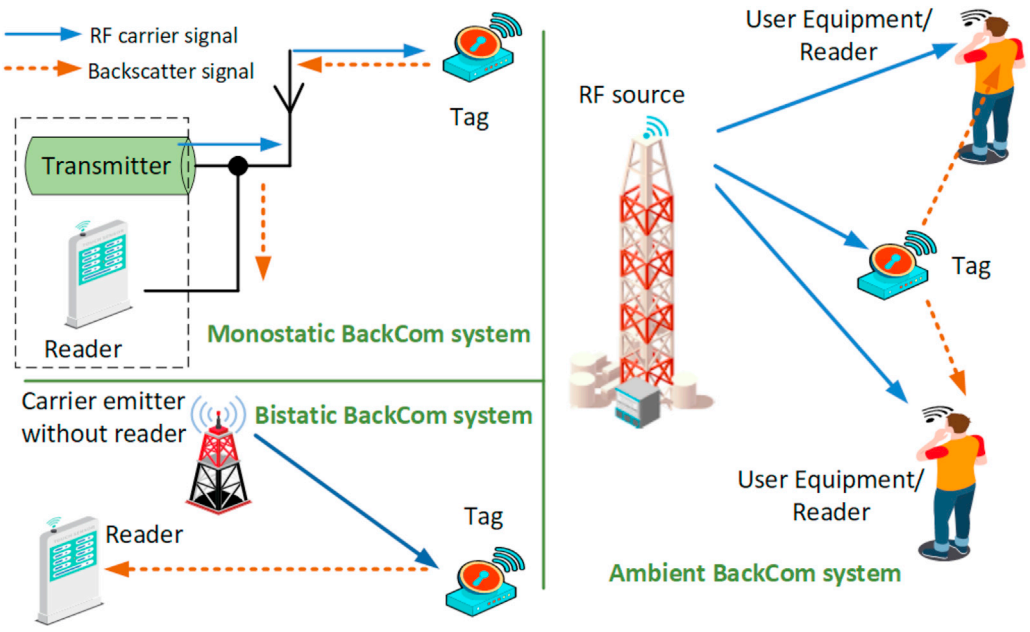

Fig. 1. Types of BackCom systems.

backscatter tag [20]. For the case of mono-static BackCom, the RF source and reader are collocated. The carrier emitted by the RF source is reflected by the backscatter tag. The reflected signal is again received by the reader at the RF source, which decodes the information. This principle of BackCom is used in the Radio Frequency Identification (RFID) tags. Nonetheless, several other customized solutions of BackCom have been proposed as a result of the gradual evolution of this technology [21]. One of the more improved versions is bistatic BackCom, which allows efficient communication when RF source and reader are not co-located. Another improved variant is ambient BackCom, which provides a more robust spectrum utilization by removing the need for a dedicated RF source [22]. Specifically, the ambient BackCom enables the exploitation of available RF signals. By proper implementation, the ambient BackCom removes the need for a dedicated RF source [23]. This feature makes ambient BackCom use spectrum and energy-constrained Internet of Things more efficiently in future communication networks. However, this also brings some complexity in the hardware design of the backscatter tag and the receiver [24]. Fig. 1 shows different types of BackCom systems.

1.1. Literature review

Recently, researchers have studied BackCom in both OMA and NOMA networks. For example, the authors in Ref. [25] have used an optimization technique to enhance the throughput of OMA BackCom network. Guo et al. [26] have optimized the successive decoding rate of the OMA BackCom system. The work in Ref. [27] has investigated the trade-off between energy and spectral efficiency of the BackCom system. Jameel et al. [28] have studied the applications of BackCom in the health-care system. The authors of [29] have proposed a technique for physical layer security of the cognitive BackCom system. Tao et al. [30] have proposed a new interference cancellation technique for OMA BackCom to investigate the bit error rate of the system. Ref. [31] has provided an efficient resource management approach to improve the energy efficiency of mobile edge computing BackCom network. Wang et al. [32] have designed an energy efficiency BackCom system by optimizing the backscatter tag's reflection coefficient. Moreover, the work in Ref. [33] has optimized the power splitting and time switching for BackCom to investigate the rate-energy trade-off. The work in Ref. [34] has also provided learning-based resource allocation in heterogeneous BackCom network. Besides, the researchers of [35–37] have also studied various applications of OMA BackCom in wireless networks. In particular [35], has discussed time slot management in BackCom [36], has studied physical layer security for BackCom, and [37] has considered multi-tone backscatter BackCom, respectively.

Despite extensive research efforts, the studies on NOMA BackCom are still in their nascent stage. In this regard, most of the studies evaluate the performance evaluation aspect of such systems. For instance, the authors of [38] have provided an outage analysis of the NOMA BackCom system. Guo et al. [39] have used NOMA for both fading-less and faded BackCom scenarios. Besides, they also provided closed-form expressions of successfully decoded bits. In Ref. [40], a new optimization framework has been proposed for Unmanned Aerial Vehicles (UAVs) and NOMA BackCom to reduce the power consumption of UAVs while improving the number of successive decided bits. For the case of multiple-input single-input, the authors of [41] have investigated the outage analysis of the NOMA BackCom system. In another study [42], Li et al. have focused on the secrecy-rate of the BackCom network. To improve the sum-rate, the work in Ref. [43] has jointly optimized the reflection coefficient and time allocation of the NOMA BackCom network. In a similar study [44], the authors have provided a novel approach to enhance the spectral efficiency and outage probability of the NOMA BackCom systems. Zhang et al. [45] have explored the outage analysis of the BackCom system. Ref. [46] studied a secrecy optimization problem of BackCom in a multi-cell NOMA network. To enhance the physical layer security, the authors of [47] have calculated the transmit power and reflection coefficient in the NOMA BackCom system. The work of Jameel et al. [48] has proposed a reliable power allocation scheme for interference management in backscatter heterogeneous networks using reinforcement learning. Moreover, the studies of [49,50] have optimized the spectral efficiency of the NOMA BackCom system under the perfect and imperfect Channel State Information (CSI) assumption. Recently, Khan et al. [51] have provided a new BackCom framework for the NOMA vehicle-to-all network. In addition,

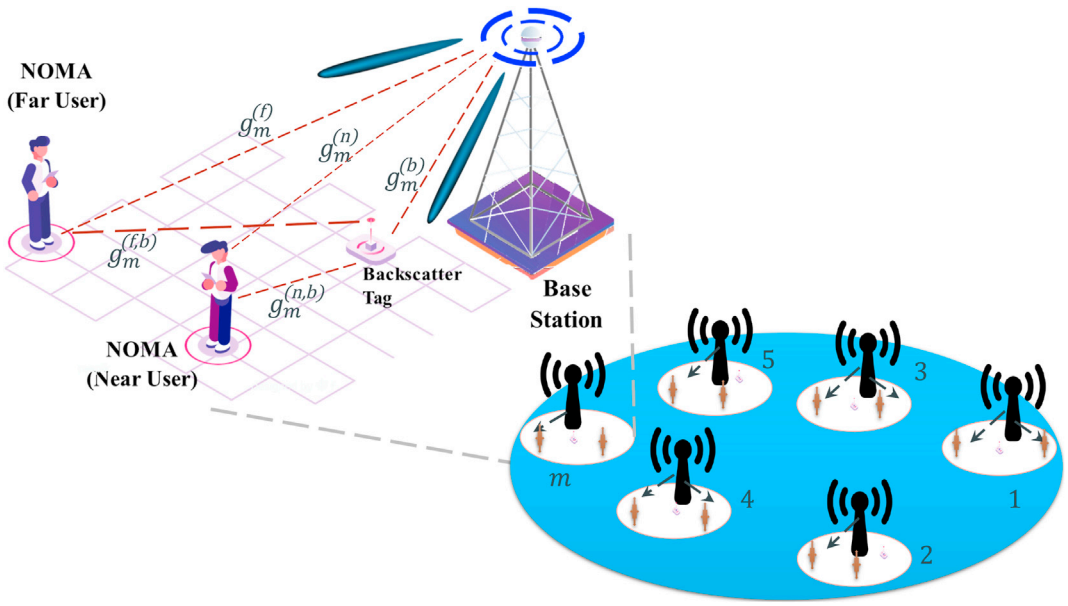

Fig. 2. System model of multi-cell NOMA Ambient BackCom network.

researchers have also investigated energy efficiency optimization problems in NOMA BackCom networks [52–54].

1.2. Motivation and contributions

It is evident from the aforementioned discussion that NOMA BackCom is slowly maturing as a feasible technology for the massive connectivity of low-powered devices. It can also be observed that most studies have considered single cell scenarios. However, there is still room for improvement before the widespread adoption of BackCom. In this regard, it is critical to evaluate the performance of NOMA BackCom in the multi-cell environment. Such studies may also help in mitigating the impact of inter-cell interference on NOMA BackCom through robust optimization techniques. In this context, our article provides the following novel contributions:

1. A multi-cell NOMA BackCom architecture has been considered, where user equipments in each cell communicate over the same frequency band using NOMA protocol. The backscatter tag utilizes the superimposed RF signal to reflect its data to nearby NOMA users.
2. An optimization framework has been developed to maximize the sum-rate of the network. The original non-convex optimization problem has been decoupled into two subproblems for finding the optimal Base Station (BS) transmitting power and backscatter reflection coefficient. The subproblems are then solved using the dual decomposition approach.
3. A comprehensive comparison of the proposed NOMA BackCom framework has been provided with pure NOMA and OMA BackCom frameworks. Results show the significant improvement in the sum-rate of the system using proposed NOMA BackCom over the benchmark pure NOMA as well as conventional OMA systems.

The remainder of the article is structured as follows. Section II discusses the system model of multi-cell network. Section III provides the problem formulation and various steps of the BS power allocation and backscatter reflection coefficient optimization techniques. In Section IV, the performance evaluation is presented along with a discussion of the results. Section V highlights the conclusions of the work and possible future research directions.

2. System and channel models

A downlink multi-cell BackCom[1] network is considered as shown in Fig. 2. In the considered model, the BS is assumed to be located at the center of each cell and communicates with two user devices using NOMA protocol. Practically, user devices in the same cell have various channel conditions; thus, we consider that the user device located near the BS has stronger channel gain than that far away from the BS [55]. For better spectrum utilization, we also assume that all the BSs are sharing the same frequency [56]. The set of BSs can be denoted as $\mathcal{M} = \{m|1,2,3,\ldots,M\}$, where m indexes m-th BS. The proposed system also consists of B uniformly distributed backscatter tags, where b indexes b-th backscatter tag and $\mathcal{B} = \{b|1,2,3,\ldots,B\}$ represents the set of backscatter tags, respectively. The channel information of user devices in each cell is available at their serving BS [57]. A single-input single-output case is considered, where all the devices are equipped with omni-directional antenna. A backscatter tag in each cell also simultaneously receives the RF signal from the BS. It harvests some energy from the RF signal and then reflects it towards user devices by adding its own information. According to the downlink NOMA protocol, the near user device can apply SIC to subtract the information of weak user device before decoding its own information [42,58]. In the end, the far user device will not apply SIC and decode its information by treating the signal of near user device as noise. The superimposed signal of m-th BS for the near user device and the far user device is denoted as x_m and can be given as

$$x_m = \sqrt{P_m \omega_m} z_m^{(n)} + \sqrt{P_m(1-\omega_m)} z_m^{(f)} \tag{1}$$

where $z_m^{(n)}$ and $z_m^{(f)}$ are the transmitted symbols of m-th BS for the near user device (denoted as n-th) and the far user device (stated as f-th), respectively. Furthermore, P_m is the power budget of m-th BS and $0 < \omega_m < 0.5$ represents the power allocation coefficient of m-th BS. According to power-domain NOMA, the m-th BS allocates more transmitting power to the f-th user device compared to the n-th user device to ensure the successful operation of SIC at the receiver side [59]. As discussed earlier, the b-th backscatter tag modulates s_m symbol, i.e., $\mathbb{E}[|s_m|^2] = 1$, and reflects it

[1] The term BackCom in this paper refers to ambient BackCom; however, the full name is omitted here for the sake of simplicity.

towards user devices. Thus, n-th user device receives the following signal:

$$y_m^{(n)} = g_m^{(n)} x_m + \sqrt{\alpha_m^{(b)}}\, g_m^{(b)} x_m g_m^{(n,b)} s_m + \sum_{m'=1, m' \neq m}^{M} h_{m'}^{(n)} \sqrt{P_{m'}}\, x_{m'} + \beta_m^{(n)} \tag{2}$$

where $g_m^{(b)}$ and $g_m^{(n)}$ are the channel gains from the BS to the near user device and backscatter tag, while $g_m^{(n,b)}$ is the channel gain from the backscatter tag to near user device. Similarly, $h_{m'}^{(n)}$ is the interference channel gain from the neighboring BS to the near user device, $P_{m'}$ denotes the interference power of neighboring BS, and $x_{m'}$ represents the data symbol of neighboring BS. Moreover, the term $\alpha_m^{(b)}$ represents the reflection coefficient of the backscatter tag and $\beta_m^{(n)}$ is the zero mean Additive White Gaussian Noise (AWGN) with variance σ^2.

Considering the effect of double fading, the signal of backscatter tag is very weaker compared to the signal of BS. Therefore, n-th user device needs to apply SIC to decode and remove its own signal as well as the signal of f-th user device from m-th BS before decoding its desired signal from the backscatter tag. Thus, the Signal to Interference plus Noise Ratio (SINR) at n-th user device for decoding the signal of f-th user device can be stated as

$$\gamma_m^{(n,f)} = \frac{|g_m^{(n)}|^2 P_m (1-\omega_m)}{P_m \omega_m (|g_m^{(n)}|^2 + |g_m^{(n,b)}|^2 \alpha_m^{(b)} |g_m^{(b)}|^2) + \ell_m^{(n)} + \sigma^2} \tag{3}$$

where $\ell_m^{(n)} = \sum_{m'=1, m' \neq m}^{M} P_{m'} |h_{m'}^{(n)}|^2$ is the interference from other BSs. After removing $z_m^{(f)}$, the n-th user device decodes its own signal. Therefore, the SINR of n-th user device to decode its own signal can be given as

$$\gamma_m^{(n,n)} = \frac{|g_m^{(n)}|^2 P_m \omega_m}{(|g_m^{n,b}|^2 \alpha_m^{(b)} |g_m^{(b)}|^2)(1-\omega_m) P_m + \ell_m^{(n)} + \sigma^2} \tag{4}$$

Finally, n-th user device decodes the signal received from the b-th backscatter tag. Thus, the SINR of n-th user device for decoding the signal from the backscatter tag can be derived as

$$\gamma_m^{n,b} = \frac{|g_m^{(n,b)}|^2 \alpha_m^{(b)} |g_m^{(b)}|^2 (P_m \omega_m + P_m (1-\omega_m))}{\ell_m^{(n)} + \sigma^2} \tag{5}$$

Accordingly, the received signal of n-th user device in m-th cell can be given as

$$y_m^{(f)} = g_m^{(f)} x_m + \sqrt{\alpha_m^{(b)}}\, g_m^{(b)} x_m g_m^{(f,b)} s_m + \sum_{m'=1, m' \neq m}^{M} h_{m'}^{(f)} \sqrt{P_{m'}}\, x_{m'} + \beta_m^{(f)} \tag{6}$$

where $g_m^{(f)}$ and $g_m^{(f,b)}$ show the channel gains from m-th BS to f-th user device and from b-th backscatter tag to f-th user device associated with m-th BS, respectively. As such, $h_{m'}^{(f)}$ is the interference channel gain from m'-th BS to f-th user device in m-th cell. Finally, the term $\beta_m^{(f)}$ is the zero mean AWGN with variance σ^2. It is important to note that f-th user device in m-th cell decodes its own signal with the interference of n-th user device and b-th backscatter tag. Thus, the SINR of f-th user device to decode its desired signal can be stated as

$$\gamma_m^{(f,f)} = \frac{|g_m^{(f)}|^2 P_m (1-\omega_m)}{P_m \omega_m (|g_m^{(f)}|^2 + |g_m^{(f,b)}|^2 \alpha_m^{(b)} |g_m^{(b)}|^2) + \ell_m^{(f)} + \sigma^2} \tag{7}$$

where $\ell_m^{(f)} = \sum_{m'=1, m' \neq m}^{M} P_{m'} |h_{m'}^{(f)}|^2$ denotes the interference from all other BSs.

3. Problem formulation and proposed solutions

In this section, we discuss different formulation steps for the sum-rate maximization problem followed by the closed-form solutions for the BS transmitting power and backscatter tag reflection coefficients. Then, we also present the proposed algorithm and complexity analysis.

3.1. Problem formulation

In this work, we evaluate the system performance by maximizing the sum-rate of the multi-cell BackCom network. In particular, the rate of user devices from BSs and backscatter tags to user devices. The total rate of the backscatter multi-cell network can be formulated as

$$R_{tot} = \sum_{m=1}^{M} (R_m^{(n,n)} + R_m^{(f,f)} + R_m^{(n,b)}), \ \forall n, \forall f, \forall b \tag{8}$$

where $R_m^{(n,n)}$, $R_m^{(f,f)}$, and $R_m^{(n,b)}$ are the rates of n-th user device from m-th BS, the rate of f-th user device from the m-th BS, and the rate of n-th user device from b-th backscatter tag in m-th cell,[2] respectively. Moreover, these rates can be given as follows:

$$R_m^{(n,n)} = \log_2(1 + \gamma_m^{(n,n)}) \tag{9}$$

$$R_m^{(f,f)} = \log_2(1 + \gamma_m^{(f,f)}) \tag{10}$$

$$R_m^{(n,b)} \approx \log_2(1 + \gamma_m^{(n,b)}) \tag{11}$$

The target of total rate maximization can be attained by user device's transmit power optimization as well as the optimization of reflection coefficient of backscatter tags. This optimization framework is subject to the reflection coefficients of backscatter tags and the transmit power of BSs according to the NOMA protocol.³ Mathematically, an optimization problem can be formulated to maximize the sum-rate of the multi-cell BackCom network as

$$\begin{aligned} \text{OP} \quad & \underset{\omega_m, \alpha_m^{(b)}}{\text{Maximize}} \ R_{tot} \\ \text{s.t.} \quad C1: \ & 0 \leq \alpha_m^{(b)} \leq \alpha_{max}, \ \forall m, \forall b \\ C2: \ & P_m \omega_m \leq P_m (1-\omega_m), \ \forall m \\ C3: \ & 0 \leq P_m \leq P_{max}, \ \forall m \\ C4: \ & 0 \leq \omega_m \leq 0.5, \ \forall m \end{aligned} \tag{12}$$

where constraint $C1$ limits the reflection coefficient between 0 and $\alpha_{\max}$, and $\alpha_{\max}$ is the maximum coefficient power that b-th backscatter tag can reflect the superimposed signal. Constraints $C2$ and $C4$ bound BSs to transmit power according to NOMA principle. In addition, $C3$ limits each BS transmit power, where $P_{\max}$ shows the BS's maximum transmission power threshold.

The above formulated optimization problem of sum-rate is non-convex [62]. Moreover, it also coupled BS power allocation and backscatter tag reflection coefficient selection, which is very complex and difficult to solve. The complexity of the original problem is reduced by first decoupling it into two subproblems for allocating optimal power at

[2] It is difficult to calculate the exact capacity of BackCom in practice [60]. Thus, a common approach is to approximate the maximum achievable capacity [25,61].

[3] Due to the weak signal of BackCom [38], the interference from backscatter tag to the far user device is almost non-existent and brings negligible change in its performance.

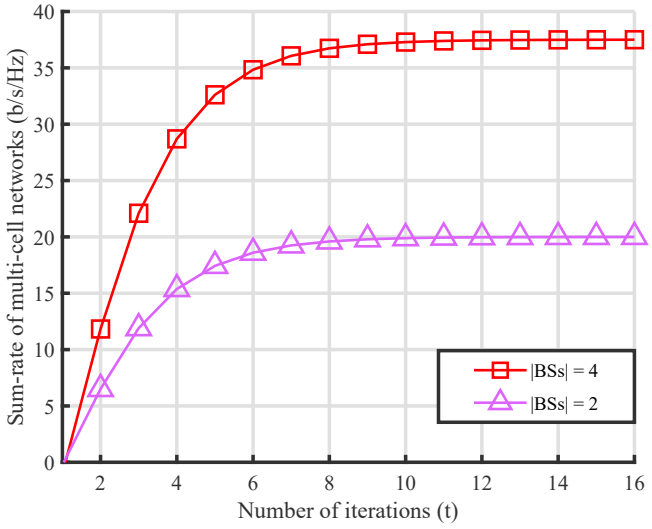

Fig. 3. Sum-rate of the proposed multi-cell NOMA BackCom versus number of iterations.

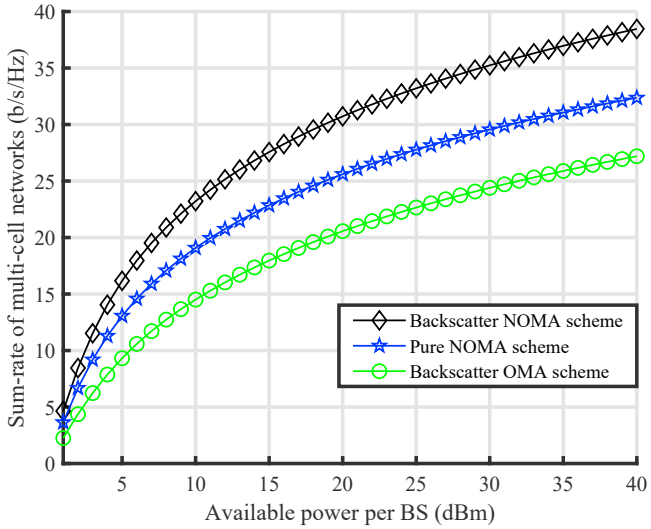

Fig. 4. Sum-rate of multi-cell BackCom versus available transmit power at each BS.

BSs and finding optimal reflection coefficient at backscatter tags. And then suboptimal techniques are provided to get the efficient solutions.

3.2. Power allocation at BSs for the given reflection coefficient of backscatter tags

Here we assume that the reflection coefficients of backscatter tags are fixed, and accordingly, the subproblem (OP1) can be formulated as

$$\begin{aligned} &\text{OP1} \quad \underset{\omega_m}{\text{Maximize}}\ R_{tot} \\ &\text{s.t.} \quad (C2)-(C4) \end{aligned} \tag{13}$$

To solve the Optimization Problem (OP1) efficiently, we adopt dual theory [63], where the dual-problem of OP1 can be derived as

$$\underset{\mu_m,\tau_m,\eta_m}{\text{Minimize}}\ \Delta(\mu_m,\tau_m,\eta_m) \tag{14}$$

where $\Delta(.)$ is the dual-function, while the dual variables including μ_m, τ_m, and η_m. $\Delta(.)$ can be written as

$$\Delta(\mu_m,\tau_m,\eta_m) = \underset{\omega_m}{\text{Maximize}}\ \mathcal{L}(\omega_m,\mu_m,\tau_m,\eta_m) \tag{15}$$

where $\mathcal{L}(\omega_m,\mu_m,\tau_m,\eta_m)$ represents Lagrangian function of OP1 and can be defined as

$$\begin{aligned} \mathcal{L}(.) \quad &= R_{tot} - \sum_{m=1}^{M}\mu_m(P_m\omega_m - P_m(1-\omega_m)) \\ &\quad -\tau_m(P_m - P_{max}) - \eta_m(\omega_m - 0.5) \end{aligned} \tag{16}$$

By expanding R_{tot}, it can be written as

$$\begin{aligned} \mathcal{L}(.) \quad &= \sum_{m=1}^{M}(R_m^{(n,n)} + R_m^{(f,f)} + R_m^{(n,b)}) \\ &\quad -\mu_m(P_m\omega_m - P_m(1-\omega_m)) \\ &\quad -\tau_m(P_m - P_{max}) - \eta_m(\omega_m - 0.5) \end{aligned} \tag{17}$$

Now, we adopt the KKT conditions to calculate a closed-form solution for ω_m as

$$\begin{aligned} \frac{\partial\mathcal{L}(.)}{\partial\omega_m} = \frac{\partial}{\partial\omega_m}\big[&\log_2(1+\gamma_m^{(n,n)}) + \log_2(1+\gamma_m^{(f,f)}) \\ &+\log_2(1+\gamma_m^{(n,b)}) - \mu_m(P_m\omega_m - P_m(1-\omega_m)) \\ &-\tau_m(P_m - P_{max}) - \eta_m(\omega_m - 0.5)\big] = 0 \end{aligned} \tag{18}$$

Substituting the values of $\gamma_m^{(n,n)}$, $\gamma_m^{(f,f)}$, and $\gamma_m^{(n,b)}$ in (18), we can obtain as (19) at the top of the next page. Considering the approximation of a high signal to noise ratio [64] and using the log properties, (19) can be rewritten as (20) mentioned at the top of the next page.

After calculating partial derivatives of (20), we obtain (21) at the top of the next page. Now we calculate the Least Common Multiple (LCM) of (21) and arrive at (22), written at the top of the next page. By setting $\mu_m P_m = 0$ and then solving for ω_m, it results in ω_m^* as

$$\begin{aligned} \frac{\partial\mathcal{L}(.)}{\partial\omega_m} = \frac{\partial}{\partial\alpha}\Bigg[&\log_2\left(1+\frac{|g_m^{(n)}|^2P_m(1-\omega_m)}{|g_m^{(n)}|^2P_m\omega_m+|g_m^{(n,b)}|^2\alpha_m^{(b)}|g_m^{(b)}|^2P_m+\ell_m^{(n)}+\sigma^2}\right) \\ &+\log_2\left(1+\frac{|g_m^{(f)}|^2P_m(1-\omega_m)}{|g_m^{(f)}|^2P_m\omega_m+|g_m^{(f,b)}|^2\alpha_m^{(b)}|g_m^{(b)}|^2P_m+\ell_m^{(f)}+\sigma^2}\right) \\ &+\log_2\left(1+\frac{|g_m^{(n,b)}|^2\alpha_m^{(b)}|g_m^{(b)}|^2P_m}{\ell_m^{(n)}+\sigma^2}\right) - \mu_m(P_m\omega_m - P_m(1-\omega_m)) - \eta_m(\omega_m - 0.5)\Bigg] = 0 \end{aligned} \tag{19}$$

$$\begin{aligned} \frac{\partial\mathcal{L}(.)}{\partial\omega_m} = \frac{\partial}{\partial\omega_m}\big[&\log_2(|g_m^{(n)}|^2P_m(1-\omega_m)) - \log_2(|g_m^{(n)}|^2P_m\omega_m + |g_m^{(n,b)}|^2\alpha_m^{(b)}|g_m^{(b)}|^2P_m + \ell_m^{(n)} + \sigma^2) \\ &+\log_2(|g_m^{(f)}|^2P_m(1-\omega_m)) - \log_2(|g_m^{(f)}|^2P_m\omega_m + |g_m^{(f,b)}|^2\alpha_m^{(b)}|g_m^{(b)}|^2P_m + \ell_m^{(f)} + \sigma^2) \\ &+\log_2(|g_m^{(n,b)}|^2\alpha_m^{(b)}|g_m^{(b)}|^2P_m) - \log_2(\ell_m^{(n)} + \sigma^2) - \mu_m(P_m\omega_m - P_m(1-\omega_m)) \\ &-\eta_m(\omega_m - 0.5)\big] = 0 \end{aligned} \tag{20}$$

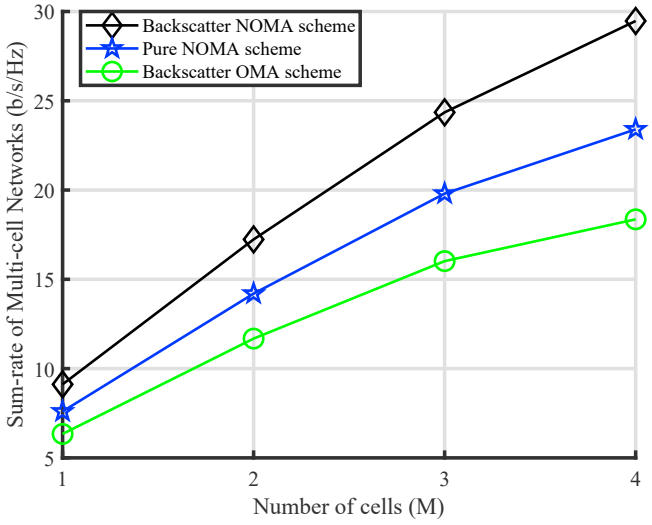

Fig. 5. Sum-rate of multi-cell BackCom versus number of cells in the network.

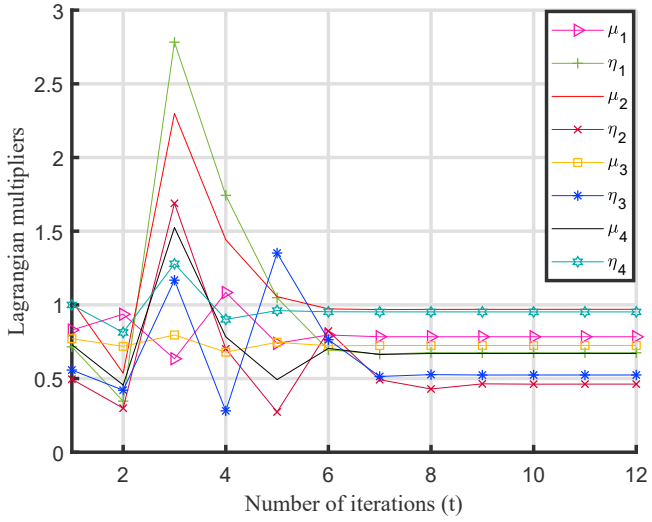

Fig. 6. Plot of the number of iterations versus Lagrangian multipliers of the NOMA BackCom scheme.

$$\frac{\partial \mathcal{L}(.)}{\partial \omega_m} = \frac{|g_m^{(f)}|^2 P_m}{|g_m^{(n)}|^2 P_m \omega_m} - \frac{|g_m^{(f)}|^2 P_m}{|g_m^{(f)}|^2 P_m \omega_m + |g_m^{(f,b)}|^2 \alpha_m^{(b)} |g_m^{(b)}|^2 P_m + \ell_m^{(f)} + \sigma^2} - \mu_m P_m - \eta_m = 0 \tag{21}$$

$$\frac{(|g_m^{(n)}|^2 P_m)(|g_m^{(f)}|^2 P_m \omega_m + |g_m^{(f,b)}|^2 \alpha_m^{(b)} |g_m^{(b)}|^2 P_m + \ell_m^{(f)} + \sigma^2) - (|g_m^{(f)}|^2 P_m)(|g_m^{(f)}|^2 P_m \omega_m)}{(|g_m^{(n)}|^2 P_m \omega_m)(|g_m^{(f)}|^2 P_m \omega_m + |g_m^{(f,b)}|^2 \alpha_m^{(b)} |g_m^{(b)}|^2 P_m + \ell_m^{(f)} + \sigma^2)} - \eta_m = \mu_m P_m \tag{22}$$

$$\omega_m^* = \left[\frac{-B_m \pm \sqrt{B_m^2 - 4A_m C_m}}{2A_m} \right]^+ \tag{23}$$

where $(\chi)^+ = \max(0, \chi)$, and the values of A_m and B_m are given by

$$A_m = |g_m^{(n)}|^2 |g_m^{(f)}|^2 P_m^2 \tag{24}$$

$$B_m = |g_m^{(n)}|^2 |g_m^{(f,b)}|^2 \alpha_m^{(b)} |g_m^{(b)}|^2 P_m^2 + |g_m^{(n)}|^2 P_m \ell_m^{(f)} + |g_m^{(f)}|^2 P_m \sigma^2 + \frac{|g_m^{(f)}|^4 P_m^2 \sigma^2 - |g_m^{(n)}|^2 |g_m^{(f)}|^2 P_m^2}{\mu_m P_m + \eta_m} \tag{25}$$

$$C_m = -\frac{|g_m^{(n)}|^2 |g_m^{(f,b)}|^2 |g_m^{(b)}|^2 P_m^2 \alpha_m^{(b)} + |g_m^{(n)}|^2 P_m \ell_m^{(f)} + |g_m^{(n)}|^2 P_m \sigma^2}{\eta_m} \tag{26}$$

while the value of C_m is provided in (26) on the next page.

At the end, η_m and μ_m are iteratively calculated as [65]

$$\eta_m(1+t) = \eta_m(t) + \delta(t)(P_m \omega_m - P_m(1-\omega_m)) \ \forall i,j,m, \tag{27}$$

$$\mu_m(1+t) = \mu_m(t) + \delta(t)(\omega_m - 0.5), \ \forall i,j,m \tag{28}$$

where t represents the iterations and δ indicates the step size. In each index of t, we find optimal values of μ_m^* and η_m^* using the computed value of ω_m. Then, in further iterations, the values of μ_m^* as well as η_m^* are utilized to obtain optimal ω_m^*. This process is stopped on convergence.

3.3. Calculating reflection coefficient at backscatter tags for the available transmit power of BSs

Now we find the reflection coefficient of backscatter tag for a given power allocation at BS. To do so, the Original Problem (OP) should be simplified as

$$\begin{aligned} &\text{OP2} \quad \underset{\alpha_m^{(b)}}{\text{Maximize}} \ R_{tot} \\ &\text{s.t.} \quad (C1) \end{aligned} \tag{29}$$

This optimization problem OP2 is convex with respect to $\alpha_m^{(b)}$. Thus, similar to the solution of P1, we exploit dual theory. The corresponding dual problem can be formulated as

$$\underset{\lambda_m}{\text{Minimize}} \ \Delta(\lambda_m) \tag{30}$$

where $\Delta(.)$ in (30) represents the dual-function, and λ_m is a dual-variable. The dual-function can be written as

$$\Delta(\lambda_m) = \underset{\lambda_m}{\text{Minimize}} \ \mathcal{L}(\alpha_m^{(b)}, \lambda_m) \tag{31}$$

where $\mathcal{L}(\alpha_m^{(b)}, \lambda_m)$ represents the Lagrangian-function shown in OP2, which can be derived as

$$\mathcal{L}(.) = R_{tot} - \lambda_m(\alpha_m^{(b)} - \alpha_{max}) \tag{32}$$

By expanding R_{tot}, it can be written as

$$\begin{aligned}\mathcal{L}(.) &= \sum_{m=1}^{M}(R_m^{(n,n)} + R_m^{(f,f)} + R_m^{(n,b)}) \\ &\quad -\lambda_m(\alpha_m^{(b)} - \alpha_{max})\end{aligned} \tag{33}$$

To obtain closed-form expression for $\alpha_m^{(b)}$, Karush-Kuhn-Tucker (KKT) conditions can be used, thus resulting in the following equations:

$$\begin{aligned}\frac{\partial\mathcal{L}(.)}{\partial\alpha_m^{(b)}} &= \frac{\partial}{\partial\alpha_m^{(b)}}\left[\log_2(1+\gamma_m^{(n,n)})\right. \\ &\quad +\log_2(1+\gamma_m^{(f,f)}) + \log_2(1+\gamma_m^{(n,b)}) \\ &\quad \left. -\lambda_m(\alpha_m^{(b)} - \alpha_{max})\right] = 0\end{aligned} \tag{34}$$

By substituting the values of $\gamma_m^{(n,n)}$, $\gamma_m^{(f,f)}$, and $\gamma_m^{(n,b)}$ in (34), we arrive at

$$\begin{aligned}\frac{\partial\mathcal{L}(.)}{\partial\alpha_m^{(b)}} &= \frac{\partial}{\partial\alpha_m^{(b)}}\left[\log_2(|g_m^{(n)}|^2P_m(1-\omega_m)) - \log_2(|g_m^{(n)}|^2P_m\omega_m + |g_m^{(n,b)}|^2\alpha_m^{(b)}|g_m^{(b)}|^2P_m + \ell_m^{(n)} + \sigma^2)\right. \\ &\quad +\log_2(|g_m^{(f)}|^2P_m(1-\omega_m)) - \log_2(|g_m^{(f)}|^2P_m\omega_m + |g_m^{(f,b)}|^2\alpha_m^{(b)}|g_m^{(b)}|^2P_m + \ell_m^{(f)} + \sigma^2) \\ &\quad \left. + \log_2(|g_m^{(n,b)}|^2\alpha_m^{(b)}|g_m^{(b)}|^2P_m) - \log_2(\ell_m^{(n)} + \sigma^2) - \lambda_m(\alpha_m^{(b)} - \alpha_{max})\right] = 0\end{aligned} \tag{36}$$

$$\begin{aligned}\frac{\partial\mathcal{L}(.)}{\partial\alpha_m^{(b)}} &= \frac{|g_m^{(n,b)}|^2|g_m^{(b)}|^2P_m}{|g_m^{(n,b)}|^2\alpha_m^{(b)}|g_m^{(b)}|^2P_m} - \frac{|g_m^{(n,b)}|^2|g_m^{(b)}|^2P_m}{|g_m^{(n)}|^2P_m\omega_m + |g_m^{(n,b)}|^2\alpha_m^{(b)}|g_m^{(b)}|^2P_m + \ell_m^n + \sigma^2} \\ &\quad -\frac{|g_m^{(f)}|^2P_m}{|g_m^{(f)}|^2P_m\omega_m + |g_m^{(f,b)}|^2\alpha_m^{(b)}|g_m^{(b)}|^2P_m + \ell_m^{(f)} + \sigma^2} - \lambda_m = 0\end{aligned} \tag{37}$$

$$\frac{(|g_m^{(n,b)}|^2|g_m^{(b)}|^2P_m)(\kappa_m^{(n)})(\iota_m^{(f)}) - (|g_m^{(n,b)}|^2|g_m^{(b)}|^2P_m)(\pi_m^{(b)})(\iota_m^{(f)}) - (|g_m^{(f)}|^2P_m)(\pi_m^{(b)})(\kappa_m^{(n)})}{(\pi_m^{(b)})(\kappa_m^{(n)})(\iota_m^{(f)})} = \lambda_m \tag{38}$$

(35) written at the top of this page. Now considering the approximation for a high signal to noise ratio and using the property of the log, (35) can be formulated as (36).

We compute the partial derivatives of (36), which leads us to (37) at the top of this page. By computing the LCM of (37), we obtain (38), given at the top of this page. Here the values of $\pi_m^{(b)}$, $\kappa_m^{(n)}$, and $\iota_m^{(f)}$ in (38) can be written as

$$\pi_m^{(b)} = |g_m^{(n,b)}|^2\alpha_m^{(b)}|g_m^{(b)}|^2P_m$$

$$\kappa_m^{(n)} = |g_m^{(n)}|^2P_m\omega_m + |g_m^{(n,b)}|^2\alpha_m^{(b)}|g_m^{(b)}|^2P_m + \ell_m^{(n)} + \sigma^2$$

$$\iota_m^{(f)} = |g_m^{(f)}|^2P_m\omega_m + |g_m^{(f,b)}|^2\alpha_m^{(b)}|g_m^{(b)}|^2P_m + \ell_m^{(f)} + \sigma^2$$

Now calculating for $\alpha_m^{(b)}$, it results in $\alpha_m^{(b)*}$ as

$$\begin{aligned}\frac{\partial\mathcal{L}(.)}{\partial\omega_m} &= \frac{\partial}{\partial\alpha_m^{(b)}}\left[\log_2\left(1+\frac{|g_m^{(n)}|^2P_m(1-\omega_m)}{|g_m^{(n)}|^2P_m\omega_m + |g_m^{(n,b)}|^2\alpha_m^{(b)}|g_m^{(b)}|^2P_m + \ell_m^{(n)} + \sigma^2}\right)\right. \\ &\quad +\log_2\left(1+\frac{|g_m^{(f)}|^2P_m(1-\omega_m)}{|g_m^{(f)}|^2P_m\omega_m + |g_m^{(f,b)}|^2\alpha_m^{(b)}|g_m^{(g)}|^2P_m + \ell_m^{(f)} + \sigma^2}\right) \\ &\quad \left.+\log_2\left(1+\frac{|g_m^{(n,b)}|^2\alpha_m^{(b)}|g_m^{(b)}|^2P_m}{\ell_m^{(n)} + \sigma^2}\right)\right) - \lambda_m(\alpha_m^{(b)} - \alpha_{max})\Bigg] = 0\end{aligned} \tag{35}$$

$$\alpha_m^{(b)*} = \left[\frac{-E_m \pm \sqrt{E_m^2 - 4D_mF_m}}{2D_m}\right]^+ \tag{39}$$

where $(v)^+ = \max(0, v)$, and the values of D_m, E_m, and F_m are respectively presented in (40), (41) and (42) at the top of the next page.

The Lagrangian multiplier λ_m is iteratively updated as

$$D_m = |g_m^{(n,b)}|^4|g_m^{(f,b)}|^2|g_m^{(b)}|^4P_m^3 + \frac{|g_m^{(n,b)}|^4|g_m^{(b)}|^4|g_m^{(f)}|^2P_m^3}{\lambda_m} \tag{40}$$

$$\begin{aligned}E_m &= |g_m^{(n,b)}|^4|g_m^{(b)}|^2P_m^2\ell_m^{(f)} + |g_m^{(n,b)}|^4|g_m^{(b)}|^4P_m^2\sigma^2 + |g_m^{(n,b)}|^2|g_m^{(b)}|^4|g_m^{(f,b)}|^2P_m^2\sigma^2 \\ &\quad +\frac{|g_m^{(n,b)}|^2|g_m^{(b)}|^2|g_m^{(f)}|^2P_m^2}{\lambda_m} + \frac{|g_m^{(n,b)}|^2|g_m^{(b)}|^2|g_m^{(f)}|^2P_m^2\ell_m^{(n)}}{\lambda_m} + \frac{|g_m^{(n,b)}|^2|g_m^{(b)}|^2|g_m^{(n)}|^2P_m^2|g_m^{(f)}|^2\omega_m}{\lambda_m} \\ &\quad +\frac{|g_m^{(n,b)}|^4|g_m^{(b)}|^4|g_m^{(f)}|^2P_m^2\omega_m}{\lambda_m} - \frac{|g_m^{(n,b)}|^2|g_m^{(b)}|^2|g_m^{(f,b)}|^2P_m^2\sigma^2}{\lambda_m}\end{aligned} \tag{41}$$

$$F_m = |g_m^{(n,b)}|^2|g_m^{(b)}|^2|g_m^{(f)}|^2 P_m^3\omega_m + |g_m^{(n,b)}|^2|g_m^{(n)}|^2|g_m^{(b)}|^2 P_m^2\omega_m\ell_m^{(f)} - \frac{|g_m^{(n,b)}|^2|g_m^{(b)}|^2|g_m^{(f)}|^2|g_m^{(n)}|^2 P_m^3\omega_m}{\lambda_m} - \frac{|g_m^{(n,b)}|^2|g_m^{(b)}|^2 P_m^2\omega_m}{\lambda_m} \quad (42)$$

$$\lambda_m(1+t) = \lambda_m(t) + \delta(t)(\alpha_m^{(b)} - \alpha_{max}),\ \forall m\forall b \quad (43)$$

where for each index of t in (43), we find optimal λ_m^* using the computed value of $\alpha_m^{(b)}$. Then, using this value of λ_m^*, we find the optimal $\alpha_m^{(b)*}$. This process will be terminated after convergence.

3.4. Resource allocation algorithm and complexity

Algorithm 1. Proposed iterative algorithm.

Algorithm 1: Proposed iterative algorithm.

if *the iteration number is zero,* $t = 0$ **then**
- Define all the variables and parameters of the system, i.e., BSs, NOMA user devices, backscatter tags, total power of each BS, reflection coefficients of backscatter tags, noise variance, and channel gains.

else
- In the first step, the power allocation coefficient ω_m of BS in each cell is calculated for a given value of backscatter tag $\alpha_m^{(b)}$.
- **for** $m = 1 : M$ **do**
  - Find ω_m using the formula of (23) and calculate η_m and μ_m iteratively as (27) and (28).
- **end**
- Now the optimal value of BS power allocation coefficient ω_m^* is substituted in subproblem (29) first, and then find the efficient value of backscatter tag reflection coefficient $\alpha_m^{(b)}$.
- **while** *not converge* **do**
  - **for** $m = 1 : M$ **do**
    - Calculate $\alpha_m^{(b)}$ using the formula (39) and iteratively update λ_m using the formula (43).
  - **end**
- **end**
- Return ω_m^*, $\alpha_{i,k}^{(b)*}$.

end

4. Numerical results

In this section, we provide results for the proposed BackCom technique in multi-cell NOMA network. We perform link-level simulations in MATLAB and use Monte Carlo methods to obtain the average channel gains (10^4 realizations). Specifically, we evaluate the system performance by sum-rate and compare three schemes, i.e., NOMA BackCom scheme, pure NOMA technique and conventional OMA BackCom technique, respectively. Here NOMA refers to the scheme without BackCom, while OMA is the Time Division Multiple Access (TDMA) scheme. According to TDMA, each BS communicates with only one user device at a given time. Accordingly, two users can receive their signals in different time slots. The parameters used in the simulations, unless mentioned otherwise, are as follows: Rayleigh fading is used to model the channels among various devices in the system, such that $g_m^{(n)} \sim \mathcal{CN}(0, \varphi_m^{(n)})$, $g_m^{(f)} \sim \mathcal{CN}(0, \varphi_m^{(f)})$, $g_m^{(b)} \sim \mathcal{CN}(0, \varphi_m^{(b)})$, $g_m^{(n,b)} \sim \mathcal{CN}(0, \varphi_m^{(n,b)})$, $g_m^{(f,b)} \sim \mathcal{CN}(0, \varphi_m^{(f,b)})$, $h_{m'}^{(n)} \sim \mathcal{CN}(0, \varphi_{m'}^{(n)})$, and $h_{m'}^{(f)} \sim \mathcal{CN}(0, \varphi_{m'}^{(f)})$, where $\varphi = 0.1$. Moreover, all the backscatter tags and user devices are uniformly distributed among all cells. The number of cells is set as $M = 4$, the maximum power of each BS is set as $P_{\max} = 40$ dBm, and the reflection coefficient of backscatter tag is set as $0 \le \alpha_{\max} \le 1$.

The results in Fig. 3 illustrate the sum-rate achieved by the proposed multi-cell NOMA BackCom scheme against the number of iterations when the number of BSs is varied. The value of the maximum BS power budget used is $P_{\max} = 40$ dBm. The result highlights that the proposed NOMA BackCom scheme has low complexity and converges within a few iterations. For example, the sum-rate of the network for both cases remains unchanged after 10 iterations. Moreover, a system with more cells can achieve more sum-rate compared to the system with fewer cells. It is because the system with more cells can accommodate more NOMA user devices and backscatter tags.

Now we present the sum-rate provided by the NOMA BackCom scheme in the multi-cell network as compared to the pure NOMA and OMA BackCom schemes. In this regard, Fig. 4 depicts the impact of BS available power budget on the system sum-rate when setting the number of BSs as $M = 4$, and the backscatter tag's maximum reflection coefficient is considered as $\alpha_{\max} = 1$. As expected, both NOMA and OMA schemes increase the system sum-rate when the total power budget of BS is increased. It can be seen from Fig. 4 that the NOMA BackCom technique outperforms the pure NOMA and conventional OMA schemes. For instance, when the transmit power of each BS is $P_{\max} = 25$ dBm, the sum-rate of our proposed NOMA BackCom scheme is 33.2 b/s/Hz in comparison with the benchmark pure NOMA and OMA schemes, i.e., 27.77 and 22.65 b/s/Hz. Besides, the sum-rate of the proposed technique is significantly enhanced in comparison with the other two schemes in the case when the transmission power of BS is increased. This is because the proposed NOMA-based technique allocated more efficiently the extra available transmit power at BS. Moreover, the integration of BackCom with NOMA achieves significant gains.

In Fig. 5, the system sum-rate is plotted against the number of cells when the maximum power budget of each BS is $P_{\max} = 40$ dBm. The proposed NOMA BackCom scheme as well as other schemes achieve higher sum rates as the available power budget for each BS increases. However, the performance of the NOMA BackCom scheme is significantly better than the pure NOMA and OMA schemes. More specifically, if the total number of BSs are 4, the sum-rate of NOMA BackCom is 36.41 b/s/Hz. On the other hand, sum-rate achieved by the pure NOMA scheme is 30.37, and OMA scheme provides a sum-rate of 25.32. Furthermore, as the number of BSs varies from 1 to 4, the sum-rate difference between NOMA and OMA techniques is increased. It is because NOMA is able to accommodate more user devices on the same network resources. These observations show that using NOMA can significantly enhance the system performance, and OMA is limited to achieving the high demands of the next-generation network.

Last but not the least, it is important to see the convergence behavior of the Lagrangian multipliers which is involved in the solution of the proposed optimization framework. It can be seen from Fig. 6 that the values of Lagrange multipliers against the iteration number. We can see that all the Lagrangian multipliers converge within a limited number of iterations. This shows that the proposed multi-cell NOMA BackCom technique exhibits low complexity.

5. Conclusions

NOMA BackCom is gradually maturing with every year. However, the performance gains of such systems are not well-explored in the existing literature. In this regard, this article has presented a resource allocation approach to enhance the spectral efficiency of the NOMA BackCom in a multi-cell environment. More specifically, a non-convex sum-rate maximization problem has been formulated with various practical constraints. Subsequently, the problem is divided into two subproblems, i.e., optimal reflection coefficient selection and BS power allocation. Both of these problems are then solved using a duality theory approach, and the results have been compared with the conventional OMA multi-cell networks. The simulation results clearly illustrate the performance gains obtained by using our proposed optimization framework.

Although the findings in this work can make significant contributions to the state-of-the-art, our work can be extended in various ways. For example, one critical issue in NOMA BackCom is that the reflected signal

is broadcast and can be intercepted by a malicious eavesdropper in the network. To solve this issue, our work would be extended to improve the secrecy capacity and reduce the secrecy outage probability of such systems. Another challenge in NOMA BackCom in a multi-cell environment can be the appropriate selection of BS for reflecting the superimposed NOMA signal. Our optimization framework can also be extended to improve the selection of BS in a multi-cell environment. These open research topics will be investigated in the future.

Conflict of interest

The authors declare that they have no known competing financial interests or personal relationships that could have appeared to influence the work reported in this paper.

References

[1] C. De Alwis, A. Kalla, Q.V. Pham, P. Kumar, M. Liyanage, Survey on 6G frontiers: trends, applications, requirements, technologies and future research, IEEE Open Journal of the Communications Society 2 (2021) 836–886.
[2] W.U. Khan, F. Jameel, T. Ristaniemi, S. Khan, G. Sidhu, J. Liu, Joint spectral and energy efficiency optimization for downlink NOMA networks, IEEE Transactions on Cognitive Communications and Networking 6 (2) (2020) 645–656.
[3] Y. Li, H. Ma, L. Wang, S. Mao, G. Wang, Optimized content caching and user association for edge computing in densely deployed heterogeneous networks, IEEE Trans. Mobile Comput. 21 (6) (2022) 2130–2142.
[4] W. U. Khan, E. Lagunas, Z. Ali, M. A. Javed, M. Ahmed, S. Chatzinotas, B. Ottersten, P. Popovski, Opportunities for Physical Layer Security in UAV Communication Enhanced with Intelligent Reflective Surfaces, arXiv preprint arXiv:2203.16907.
[5] S. Xia, Z. Yao, Y. Li, S. Mao, Online distributed offloading and computing resource management with energy harvesting for heterogeneous MEC-enabled iot, IEEE Trans. Wireless Commun. 20 (10) (2021) 6743–6757.
[6] X. Li, J. Li, Z. Ding, A. Nallanathan, Residual transceiver hardware impairments on cooperative NOMA networks, IEEE Trans. Wireless Commun. 19 (1) (2020) 680–695.
[7] K. Dev, S.A. Khowaja, P.K. Sharma, B.S. Chowdhry, S. Tanwar, G Fortino, DDI: a novel architecture for joint active user detection and IoT device identification in grant-free NOMA systems for 6G and beyond networks, IEEE Internet Things J 9 (4) (2021) 2906–2917.
[8] O. Maraqa, A. Rajasekaran S., S. Al-Ahmadi, H. Yanikomeroglu, S. Sait, A survey of rate-optimal power domain NOMA with enabling technologies of future wireless networks, IEEE Communications Surveys Tutorials 22 (4) (2020) 2192–2235.
[9] W.U. Khan, Z.Y. Yu, S.S. Yu, G.A. Sardar, Efficient power allocation in downlink multi-cell multi-user NOMA networks, IET Commun. 13 (4) (2018) 396–402.
[10] W.U. Khan, J. Liu, F. Jameel, V. Sharma, Z. Han, Spectral efficiency optimization for next generation NOMA-enabled IoT networks, IEEE Trans. Veh. Technol. 69 (12) (2020) 15284–15297.
[11] X. Li, M. Zhao, C. Zhang, W.U. Khan, R. Kharel, Security analysis of multi-antenna NOMA networks under I/Q imbalance, Electronics 8 (11) (2019) 1327.
[12] Z. Ali, et al., Joint user pairing, channel assignment and power allocation in NOMA based CR systems, Appl. Sci. 9 (20) (2019) 4282.
[13] L. Zhu, Z Xiao, X.G. Xia, D.O. Wu, Millimeter-wave communications with non-orthogonal multiple access for B5G/6G, IEEE Access 7 (2019) 116123–116132.
[14] A. Nasser, O. Muta, M. Elsabrouty, H. Gacanin, Interference mitigation and power allocation scheme for downlink MIMO-NOMA HetNet, IEEE Trans. Veh. Technol. 68 (7) (2019) 6805–6816, https://doi.org/10.1109/TVT.2019.2918336.
[15] Y. Du, B.H. Dong, Z. Chen, X.D. Wang, Z.Y. Liu, P.Y. Gao, S.Q. li, Efficient multi-user detection for uplink grant-free NOMA: prior-information aided adaptive compressive sensing perspective, IEEE J. Sel. Area. Commun. 35 (12) (2017) 2812–2828.
[16] F. Jameel, S. Wyne, G. Kaddoum, T.Q. Duong, A comprehensive survey on cooperative relaying and jamming strategies for physical layer security, IEEE Communications Surveys Tutorials 21 (3) (2019) 2734–2771.
[17] W.U. Khan, F. Jameel, G.A.S. Sidhu, M. Ahmed, X.W. Li, R. Jäntti, Multiobjective optimization of uplink NOMA-enabled vehicle-to-infrastructure communication, IEEE Access 8 (2020) 84467–84478.
[18] Z. Ding, P. Fan, H.V. Poor, Impact of non-orthogonal multiple access on the offloading of mobile edge computing, IEEE Trans. Commun. 67 (1) (2018) 375–390.
[19] C. Xu, et al., Practical backscatter communication systems for battery-free internet of things: a tutorial and survey of recent research,, IEEE Signal Process Mag. 35 (5) (2018) 16–27.
[20] F. Jameel, et al., NOMA-enabled backscatter communications: towards Battery-free IoT Networks 4th, 3, IEEE Internet Things Mag., 2020, pp. 95–101.
[21] W. Liu, K. Huang, X. Zhou, S. Durrani, Full-duplex backscatter interference networks based on time-hopping spread spectrum, IEEE Trans. Wireless Commun. 16 (7) (2017) 4361–4377.
[22] G. Wang, F. Gao, R. Fan, C. Tellambura, Ambient backscatter communication systems: detection and performance analysis, IEEE Trans. Commun. 64 (11) (2016) 4836–4846.
[23] W.U. Khan, G. Ahmad, X. Li, Z. Kaleem, J. Liu, NOMA-enabled wireless powered backscatter communications for secure and green IoT networks, in: Wireless-Powered Backscatter Communications for Internet of Things, Springer, 2020, pp. 103–131.
[24] X.L. Cao, Z.X. Song, B. Yang, M.A. ElMossallamy, L.J. Qian, Z. Han, A distributed ambient backscatter MAC protocol for internet-of-things networks, IEEE Internet Things J. 7 (2) (2020) 1488–1501.
[25] B. Lyu, C. You, Y. Zhen, G. Guan, The optimal control policy for RF-powered backscatter communication networks, IEEE Trans. Veh. Technol. 67 (3) (2017) 2804–2808.
[26] J. Guo, X. Zhou, S. Durrani, H. Yanikomeroglu, Backscatter communications with NOMA (invited paper), in: Int. Symp. Wireless Commun. Sys., ISWCS, 2018, pp. 1–5.
[27] F. Jameel, et al., Simultaneous harvest-and-transmit ambient backscatter communications under Rayleigh fading, EURASIP J. Wirel. Commun. Netw. 2019 (1) (2019) 166.
[28] F. Jameel, R. Duan, Z. Chang, A. Liljemark, R. Jantti, Applications of backscatter communications for healthcare networks, IEEE Network 33 (6) (2019) 50–57.
[29] X. Li, Y. Zheng, W.U. Khan, M. Zeng, L. Li, Physical layer security of cognitive ambient backscatter communications for green Internet-of-things, IEEE Trans. Green Commun. Netw. 5 (3) (2021) 1066–1076.
[30] Q. Tao, Y. Li, C. Zhong, S. Shao, Z. Zhang, A novel interference cancellation scheme for bistatic backscatter communication systems, IEEE Commun. Lett. 25 (6) (2021) 2014–2018.
[31] Y. Xu, R.Q. Hu, Joint computation offloading and radio resource allocation in MEC-based wireless-powered backscatter communication networks, IEEE Trans. Veh. Technol. 70 (6) (2021) 6200–6205.
[32] Y. Wang, S. Yan, W. Wang, Y. Huang, C. Liu, Energy-efficient covert communications for bistatic backscatter systems, IEEE Trans. Veh. Technol. 70 (3) (2021) 2906–2911.
[33] G. Sacarelo, Y.H. Kim, Rate-energy tradeoffs of wireless powered backscatter communication with power splitting and time switching, IEEE Access 9 (2021) 10844–10857.
[34] W.U. Khan, T.N. Nguyen, F. Jameel, M.A. Jamshed, H. Pervaiz, M.A. Javed, R. Jantti, Learning-based resource allocation for backscatter-aided vehicular networks, IEEE Trans. Intell. Transport. Syst. (2021) 1–15.
[35] F. Jameel, et al., Time slot management in backscatter systems for large-scale IoT networks, in: Wireless-Powered Backscatter Communications for Internet of Things, Springer, pp. 51–65.
[36] A. Mehmood, W. Aman, M.M.U. Rahman, M.A. Imran, Q.H. Abbasi, Preventing identity attacks in RFID backscatter communication systems: a physical-layer approach, in: 2020 International Conference on UK-China Emerging Technologies (UCET), IEEE, 2020, pp. 1–5.
[37] F. Jameel, M. Nabeel, W.U. Khan, Multi-tone carrier backscatter communications for massive IoT networks, Wireless-Powered Backscatter Communications for Internet of Things, Springer, pp. 39–50.
[38] Q. Zhang, L. Zhang, Y.C. Liang, P.Y. Kam, Backscatter-NOMA: a symbiotic system of cellular and Internet-of-Things networks, IEEE Access 7 (2019) 20000–20013.
[39] J. Guo, X. Zhou, S. Durrani, H. Yanikomeroglu, Design of non-orthogonal multiple access enhanced backscatter communication, IEEE Trans. Wireless Commun. 17 (10) (2018) 6837–6852.
[40] A. Farajzadeh, O. Ercetin, H. Yanikomeroglu, UAV data collection over NOMA backscatter networks: UAV altitude and trajectory optimization, in: IEEE Int. Conf. Commun., ICC), 2019, pp. 1–7.
[41] C. Le, D. Do, Outage performance of backscatter NOMA relaying systems equipping with multiple antennas, IET Electron. Lett. 55 (19) (2019) 1066–1067, https://doi.org/10.1049/el.2019.1390.
[42] Y. Li, et al., Secure Beamforming in MISO NOMA Backscatter Device Aided Symbiotic Radio Networks, arXiv preprint arXiv:1906.03410.
[43] G. Yang, X. Xu, Y.C. Liang, Resource allocation in NOMA-enhanced backscatter communication networks for wireless powered IoT, IEEE Wireless Commun. Lett. 9 (1) (2020) 117–120.
[44] S. Zeb, Q. Abbas, S.A. Hassan, A. Mahmood, M. Gidlund, NOMA enhanced backscatter communication for green IoT networks, in: Int. Symp. Wireless Commun. Sys., ISWCS, 2019, pp. 1–5.
[45] Q. Zhang, L. Zhang, Y.C. Liang, P.Y. Kam, Backscatter-NOMA: an integrated system of cellular and internet-of-things networks, in: IEEE Int. Conf. Commun., ICC, 2019, pp. 1–6.
[46] W.U. Khan, J. liu, F. Jameel, M.T.R. Khan, R. Jantti, Secure backscatter communications in multi-cell NOMA networks: enabling link security for massive IoT networks, in: IEEE INFOCOM 2020-IEEE Conference on Computer Communications Workshops, IEEE, 2020, pp. 213–218.
[47] W.U. Khan, Z. Ali, A.U. Khan, G.A.S. Sidhu, Secure Backscatter-Enabled NOMA System Design in 6G Era, Internet Technology Letters (2021) e307.
[48] F. Jameel, W.U. Khan, M.A. Jamshed, H. Pervaiz, R. Jantti, Reinforcement learning for scalable and reliable power allocation in SDN-based backscatter heterogeneous network, in: IEEE INFOCOM 2020 - IEEE Conference on Computer Communications Workshops, IEEE, 2020, pp. 1069–1074.
[49] W.U. Khan, et al., Joint Optimization of NOMA-enabled backscatter communications for beyond 5G IoT networks, Internet Technol. Lett. 265 (2021), https://doi.org/10.1002/itl2.265.
[50] W.U. Khan, X. Li, M. Zeng, O.A. Dobre, Backscatter-enabled NOMA for future 6G systems: a new optimization framework under imperfect SIC, IEEE Commun. Lett. 25 (5) (2021) 1669–1672.

[51] W.U. Khan, F. Jameel, N. Kumar, R. Jäntti, M. Guizani, Backscatter-enabled efficient V2X communication with non-orthogonal multiple access, IEEE Trans. Veh. Technol. 70 (2) (2021) 1724–1735.
[52] M. Ahmed, W.U. Khan, A. Ihsan, X. Li, J. Li, T.A. Tsiftsis, Backscatter sensors communication for 6G low-powered NOMA-enabled IoT networks under imperfect SIC, IEEE Syst. J. (2022) 1–11.
[53] W.U. Khan, M.A. Javed, T.N. Nguyen, S. Khan, B.M. Elhalawany, Energy-efficient resource allocation for 6G backscatter-enabled NOMA IoV networks, IEEE Trans. Intell. Transport. Syst. 23 (7) (2022) 9775–9785.
[54] A. Ihsan, W. Chen, W.U. Khan, Energy-efficient Backscatter Aided Uplink NOMA Roadside Sensor Communications under Channel Estimation Errors, arXiv preprint arXiv:2109.05341.
[55] Z.K. Zhang, H.J. Sun, R.Q.Y. Hu, Downlink and uplink non-orthogonal multiple access in a dense wireless network, IEEE J. Sel. Area. Commun. 35 (12) (2017) 2771–2784.
[56] B. Xu, C. Yue, J.R. Carrion, T. Zhang, Resource allocation in energy-cooperation enabled two-tier NOMA HetNets toward green 5G, IEEE J. Sel. Area. Commun. 35 (12) (2017) 2758–2770.
[57] W.U. Khan, F. Jameel, X. Li, M. Bilal, T.A. Tsiftsis, Joint spectrum and energy optimization of NOMA-enabled small-cell networks with QoS guarantee, IEEE Trans. Veh. Technol. 70 (8) (2021) 8337–8342.
[58] A. Ali, A. Baig, G.M. Awan, W.U. Khan, S. Sidhu, Efficient resource management for sum capacity maximization in 5G NOMA systems, Appl. Syst. Innov. 2 (3) (2019) 27.
[59] F. Jameel, W.U. Khan, Z. Chang, T. Ristaniemi, J. Liu, Secrecy analysis and learning-based optimization of cooperative NOMA SWIPT systems, in: IEEE International Conference on Communications Workshops, IEEE, 2019, pp. 1–6.
[60] J. Qian, A.N. Parks, J.R. Smith, F.F. Gao, S. Jin, IoT communications with *M*-PSK modulated ambient backscatter: algorithm, analysis, and implementation, IEEE Internet Things J. 6 (1) (2018) 844–855.
[61] D. Li, Y.C. Liang, Adaptive ambient backscatter communication systems with MRC, IEEE Trans. Veh. Technol. 67 (12) (2018) 12352–12357.
[62] M. Chiang, Nonconvex optimization for communication networks, in: Advances in Applied Mathematics and Global Optimization, Springer, 2009, pp. 137–196.
[63] K. Bakht, F. Jameel, Z. Ali, W.U. Khan, I. Khan, G.A.S. Sidhu, J.W. Lee, Power allocation and user assignment scheme for beyond 5G heterogeneous networks, Wireless Commun, Wireless Commun. & Mobile Comput. (2019).
[64] W. Aman, G.A.S. Sidhu, H.M. Furqan, Z. Ali, Enhancing physical layer security in AF relay-assisted multicarrier wireless transmission, Trans. Emerg. Telecommun. Technol. 29 (6) (2018) e3289.
[65] W.U. Khan, X. Li, A. Ihsan, M.A. Khan, M. Ahmed, NOMA-enabled optimization framework for next-generation small-cell IoV networks under imperfect SIC decoding, IEEE Trans. Intell. Transport. Syst. (2021), 1–1.